Catalyst and processing effects on metal-assisted chemical etching for the production of highly porous GaN

2013 Semicond. Sci. Technol. 28 065001

(http://iopscience.iop.org/0268-1242/28/6/065001)

Semicond. Sci. Technol. **28** (2013) 065001 (10pp) doi:10.1088/0268-1242/28/6/065001

Catalyst and processing effects on metal-assisted chemical etching for the production of highly porous GaN

Xuewen Geng[1,2,4,5], **Barrett K Duan**[3], **Dane A Grismer**[1], **Liancheng Zhao**[2] **and Paul W Bohn**[1,3,5]

[1] Department of Chemical and Biomolecular Engineering, University of Notre Dame, Notre Dame, IN 46556, USA
[2] School of Materials Science and Engineering, Harbin Institute of Technology, No.92, West Da-Zhi Street, Harbin, Heilongjiang Province 150001, People's Republic of China
[3] Department of Chemistry and Biochemistry, University of Notre Dame, Notre Dame, IN 46556, USA

E-mail: pbohn@nd.edu and gengxuewen@gmail.com

Received 19 December 2012, in final form 22 March 2013
Published 30 April 2013
Online at stacks.iop.org/SST/28/065001

Abstract
Metal-assisted chemical etching is a facile method to produce micro-/nanostructures in the near-surface region of gallium nitride (GaN) and other semiconductors. Detailed studies of the production of porous GaN (PGaN) using different metal catalysts and GaN doping conditions have been performed in order to understand the mechanism by which metal-assisted chemical etching is accomplished in GaN. Patterned catalysts show increasing metal-assisted chemical etching activity to *n*-GaN in the order Ag < Au < Ir < Pt. In addition, the catalytic behavior of continuous films is compared to discontinuous island films. Continuous metal films strongly shield the surface, hindering metal-assisted chemical etching, an effect which can be overcome by using discontinuous films or increasing the irradiance of the light source. With increasing etch time or irradiance, PGaN morphologies change from uniform porous structures to ridge and valley structures. The doping type plays an important role, with metal-assisted chemical etching activity increasing in the order *p*-GaN < intrinsic GaN < *n*-GaN. Both the catalyst identity and the doping type effects are explained by the work functions and the related band offsets that affect the metal-assisted chemical etching process through a combination of different barriers to hole injection and the formation of hole accumulation/depletion layers at the metal–semiconductor interface.

S Online supplementary data available from stacks.iop.org/SST/28/065001/mmedia

1. Introduction

III–V compound semiconductors, particularly III-nitrides, have attracted considerable attention during the past 20 years [1–3] due to their wide direct bandgaps, low chemical reactivity [1] and stable photoelectric and mechanical properties in aggressive environments [4, 5]. The prototypical III-nitride, gallium nitride (GaN), has been widely studied due to its strong chemical bonds, radiation hardness, large breakdown voltage and other advantageous properties [6]. Various approaches have been reported to produce GaN nanostructures, notably fabrication of porous GaN (PGaN) layers, which have unique optical [5, 7–9] and mechanical characteristics, and promising advantages over other widely used materials, such as Si [3]. PGaN layers have been used in surface-enhanced Raman scattering [10], high sensitivity gas sensing [4] and as the strain-relaxed layers for the overgrowth of III-nitride devices with low dislocation density [11]. In addition, it has been used as an efficient photoanode

[4] Present address: Renewable Energy Materials Research Science & Engineering Center, Colorado School of Mines, Golden, CO 80401, USA.
[5] Authors to whom any correspondence should be addressed.

for solar-powered water splitting, converting the alternative energy source to fuel, without emitting CO_2 [12]. Furthermore, the preparation of composite nanostructures, either through metallization or chemical functionalization, can significantly enhance the potential uses of these nanoporous structures. As an example, catalytic metals, such as platinum or palladium, can be deposited in close contact with PGaN for chemical catalysis and biomolecular gas sensing [13, 14]. In addition, similar structures exhibit photon detection with high sensitivity [15, 16] when used to realize Schottky diodes on PGaN.

PGaN production approaches can be classified into two categories: dry [17] and wet etching [2, 3, 10, 11, 18–21]. The latter is advantageous, because it is a simple approach to fashion materials at nanometer length scales, and it is compatible with common industrial processes. However, wet etching of GaN to produce porous layers is still in the early stages of development [3] and is mainly focused on *n*-GaN. *n*-GaN can be etched in alkaline solution at elevated temperatures, but alkaline etches do not work well for intrinsic and *p*-GaN [10, 20]. In addition, electrochemical etching in alkaline or acidic solutions [2, 3, 11, 18, 21] can be used to produce porous *n*-GaN, when carried out in HF, activated by an external current, and with above-bandgap illumination. These factors support etching by creating electron−hole pairs, followed by oxidative dissociation of the semiconductor, a reaction that consumes photo-generated holes [19]. The morphology of the etched material is affected by electrolyte identity and concentration [18], illumination intensity, sample bias and material doping level [19].

In contrast, metal-assisted chemical etching is a simple alternative to photoelectrochemical etching that uses electroless etching to produce porous semiconductors [22]. Depending on the bandgap of the material, UV illumination may still be needed, as it is for GaN, but not for Si. Many kinds of III−V porous layers including *n*-GaAs [23] and *n*-GaN [4, 5, 7–9] have been successfully fabricated by metal-assisted chemical etching at room temperature. Previously, Raman scattering has confirmed that the chemical composition of GaN remains unchanged upon metal-assisted chemical etching, i.e. there is no preferential etching [24]. One outstanding issue, however, is the relationship of the metal catalysts and processing conditions to the morphology of the final material, which can vary depending on the spatial distribution and identity of the catalyst [22], making it difficult to obtain uniform nanostructures across the whole surface. So far, only Pt island films have been confirmed as effective catalysts for the metal-assisted chemical etching of *n*-GaN [4, 5, 7–9], and these are difficult to remove after metal-assisted chemical etching without destroying the porous structures produced. Furthermore, the detailed metal-assisted chemical etching mechanism is not well understood.

Here, metal-assisted chemical etching of GaN is studied using different metal catalysts, including Ag, Au, Ir and Pt, deposited by different methods and spatial distributions (figure 1), with varying substrate doping, etch time and illumination intensity. Based on these parametric studies, the mechanism of metal-assisted chemical etching of GaN is clarified, and conditions for optimal etching are identified.

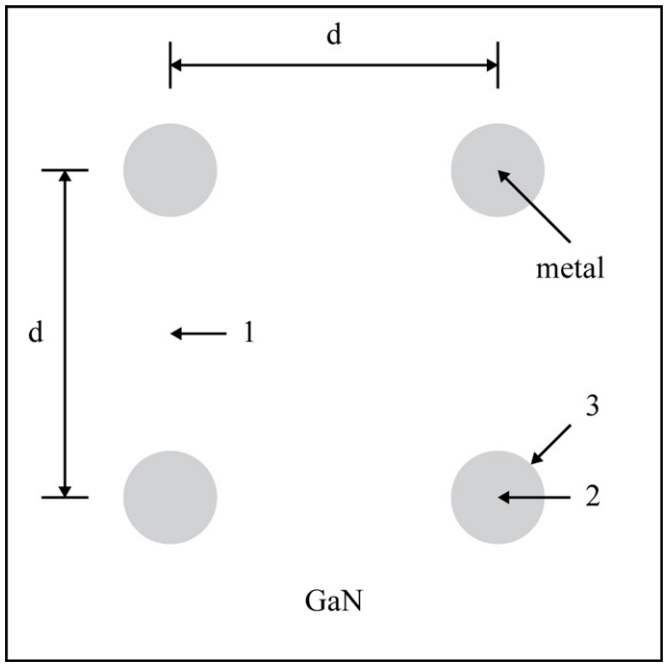

Figure 1. Noble metal patterns sputtered on clean *n*-GaN wafers used as catalysts for metal-assisted chemical etching.

2. Experimental details

2.1. Materials

GaN wafers used in the present study were N-face *n*-type GaN (10 μm thick, $[Si_{Ga}] = 10^{18}$ cm^{-3}), *p*-type GaN (10 μm thick, $[Mg_{Ga}] = 10^{18}$ cm^{-3}) and intrinsic GaN (4 μm thick), grown by hydride vapor phase epitaxy (HVPE) on (0 0 0 1) sapphire (TDI, Oxford Instruments, Inc.). Hydrochloric acid (HCl, 36.5–38% ACS grade), acetone (C_3H_6O, ACS grade) and isopropyl alcohol (IPA, $(CH_3)_2CHOH$, ACS grade) were purchased from VWR International. Nitric acid (HNO_3, 70%) was purchased from Sigma-Aldrich Co. Methanol (CH_3OH, reagent grade) and hydrogen peroxide (H_2O_2, 30%) was purchased from Fisher Scientific. Hydrofluoric acid (HF, 49% electronic grade) was purchased from Transene Co. Unless otherwise noted, all reagents were used as received. Deionized (DI) water ($\rho \sim 18.2$ MΩ cm) from a Milli-Q Gradient water purification system (Millipore) was used to prepare all aqueous solutions and for rinsing, unless otherwise noted.

2.2. Metal-assisted electroless etching

GaN substrates were cut into 1 cm^2 squares and were ultrasonically cleaned in acetone (5 min), isopropyl alcohol (5 min) and DI H_2O (5 min, three times) sequentially and then cleaned in concentrated aqua regia (3:1 HCl:HNO_3, v:v) for 30 min, followed by rinsing in DI H_2O and CH_3OH, and then drying with N_2. Metals were sputter-coated, either as islands (8 nm thickness) through an Al mask composed of 0.5 mm diameter holes, as shown in figure 1, or as continuous films (3–20 nm) with a Desk IV sputter coater (Denton Vacuum) onto GaN wafers. For comparison, Ag nanoparticle catalysts were also deposited by the silver-mirror reaction on

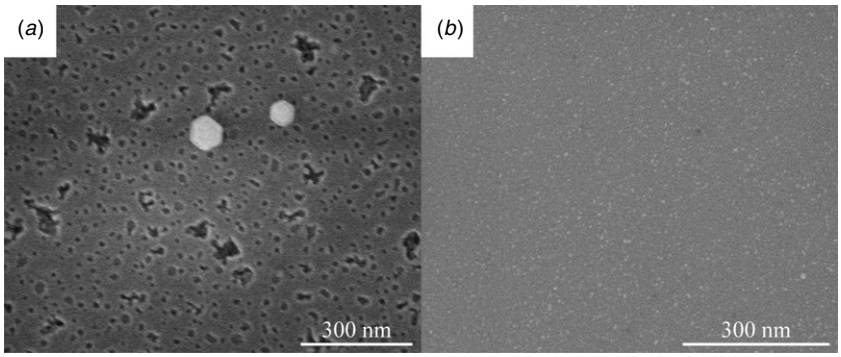

Figure 2. Top-view FESEM images of *n*-GaN wafers subjected to metal-assisted chemical etching in 2:2:1 (v:v:v) HF(49%):H_2O_2(30%): methanol at 300 K for 60 min. (*a*) Processed under 45 mW UV illumination without metal catalyst; (*b*) etched without illumination using 10 nm sputtered Ir islands as catalyst. The observed site in panel (*b*) corresponds to position 1 in figure 1.

the surface of *n*-GaN [25]. GaN substrates were etched in 2:2:1 HF:H_2O_2:CH_3OH (v:v:v) under a 100 W Hg lamp (Oriel Instruments model 6182, Oriel Instruments 68 806 power supply) for times ranging from 10 to 120 min to generate PGaN layers. The incident UV power varied from 40 to 200 mW. The samples were then rinsed thoroughly in DI water and CH_3OH and dried with N_2. The morphologies of the etched samples were characterized in plan view and cross-section by field emission scanning electron microscopy (FESEM) (FEI Magellan 400) equipped with an XFlash 5010 energy dispersive x-ray spectrometer.

3. Results and discussion

3.1. Mechanism

The detailed metal-assisted chemical etching mechanism of GaN is not known; however, it is well accepted that the N-face of GaN is unstable compared with the Ga-face [6, 26], and it can be etched under UV illumination, releasing N_2 [18, 20]. Further, under comparable conditions, the metal-assisted chemical etching rate of GaN is much smaller than Si. Possible explanations include the higher Schottky barrier height of Pt/GaN compared to Pt/Si, the slower dissolution of Ga_2O_3 relative to SiO_2 in HF [9], the wider bandgap of GaN, the carrier mobilities [27, 28], and Ga-N *versus* Si-Si bond energies [20, 29]. In the exothermic overall reaction, heat is released and soluble $GaF_2(OH)$ is produced. Based on the factors above and positing the formation of a localized galvanic cell, a mechanism consistent with all known observations is Cathode:

$$H_2O_2 + 2H^+ \rightarrow 2H_2O + 2h^+ \quad (1)$$

Anode:

$$2GaN + 6\,h^+ + 4HF + 2H_2O \rightarrow 2GaF_2(OH) + 6H^+ + N_2 \uparrow \quad (2)$$

Overall:

$$2GaN + 3H_2O_2 + 4HF \rightarrow 2GaF_2(OH) + N_2 \uparrow + 4H_2O\,. \quad (3)$$

In this mechanism, holes are produced and injected at the cathode and move from sites around the metal patterns (islands) to distal locations due to the high mobility of carriers in GaN (Table S1, Electronic Supplementary Information, ESI available at stacks.iop.org/SST/28/065001/mmedia). Once there, they participate in the anode reaction resulting in the formation of a uniform porous layer on the surface.

3.2. Morphological evolution of n-GaN with UV irradiation

In the metal-assisted chemical etching process, holes derived from the oxidation reaction must be injected into the valence band in order to drift to the sample surface and participate in the etching reaction. For wide bandgap semiconductors, like GaN, radiation is required to supply the extra energy needed for hole injection. Figure 2 compares metal-assisted chemical etching results on *n*-GaN with illumination but no catalyst, figure 2(*a*), to etching with catalyst but no irradiation, figure 2(*b*). As shown, low density nanoscale pores are produced uniformly on the surface of *n*-GaN in the presence of UV illumination, but not without it. Although the etch pits are shallow, they are distributed uniformly, and some of them begin to merge into bigger pores. No etching features are observed without illumination, even with Ir catalyst, as shown in figure 2(*b*), although vigorous bubble formation is observed. The most likely explanation for the bubbles is the common disproportionation of H_2O_2 catalyzed by transition metals, described by equation (4) [30],

$$3H_2O_2 \rightarrow 2H_2O + O_2 \uparrow\,. \quad (4)$$

3.3. Effect of catalyst proximity on morphology

The uniformity of PGaN morphology produced by metal-assisted chemical etching of *n*-GaN surface depends on the length scale observed. Although quite uniform on a nanometer length scale, morphology varies on longer length scales and also varies with position relative to the deposited catalyst features depicted in figure 1. Figures 3(*a*) and (*b*) show trench-like structures obtained at positions 1 and 3, respectively. Not surprisingly, metal-assisted chemical etching in regions adjacent to metal island features (positions 1 and 3) behaves differently than position 2, directly under the metal islands (not shown). Figure 3(*b*) shows trench-like structures obtained

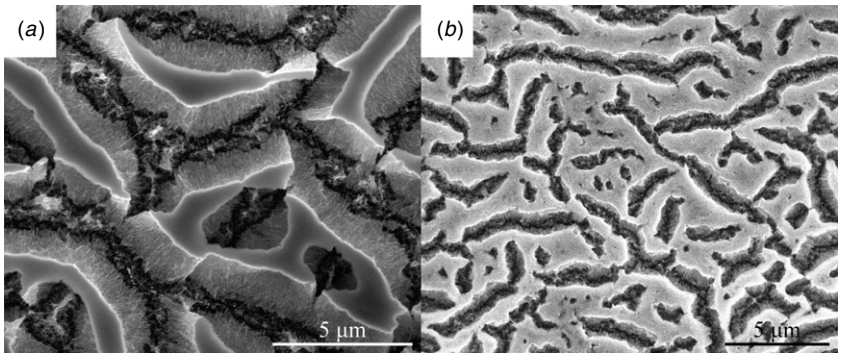

Figure 3. Top-view FESEM images of *n*-GaN wafers subjected to metal-assisted chemical etching in 2:2:1 (v:v:v) HF(49%):H_2O_2(30%): methanol at 300 K using 7 nm catalytic Ir sputtered islands. (*a*) Site 1 (figure 1) processed under 130 mW UV illumination for 45 min; (*b*) site 3 (figure 1) processed under 130 mW UV illumination for 45 min.

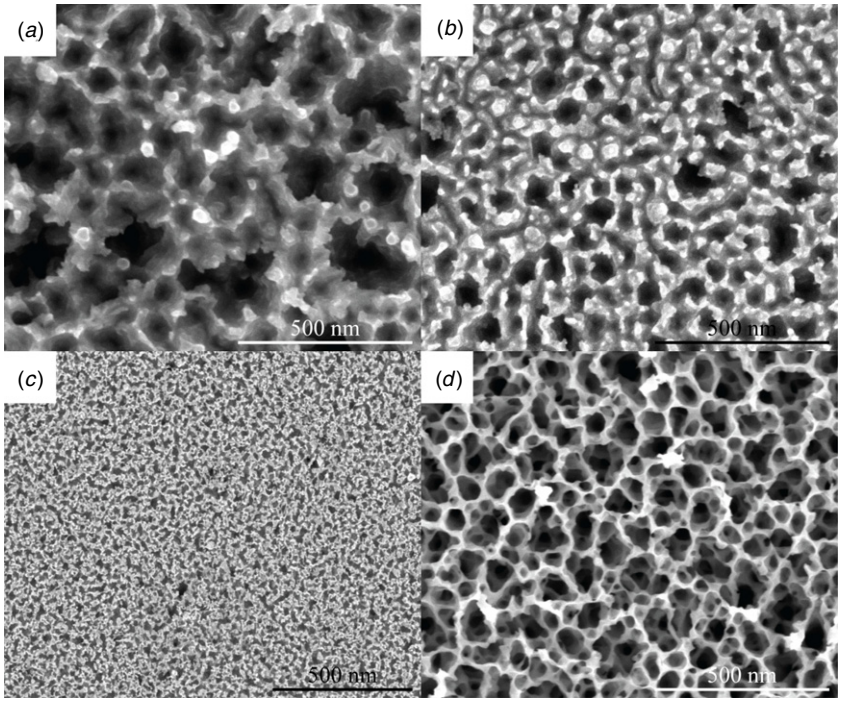

Figure 4. Top-view FESEM images of *n*-GaN wafers subjected to metal-assisted chemical etching in 2:2:1 (v:v:v) HF(49%):H_2O_2(30%): methanol at 300 K using 7 nm catalytic metal sputtered islands. The catalysts used were: (*a*) Ag processed under 90 mW UV illumination for 60 min; (*b*) Au processed under 90 mW UV illumination for 60 min; (*c*) Ir processed under 90 mW UV illumination for 10 min; (*d*) Pt processed under 90 mW UV illumination for 10 min. The observed sites correspond to position 1 in figure 1.

in position 3 that are similar to those in position 1, but at higher density. The differences can be attributed to the physical mechanism of the etching process. During metal-assisted chemical etching, holes are injected into the semiconductor area around the metals and then diffuse and/or drift away from the deposited metal regions. The availability of holes at the GaN-solution interface controls the rate of formation of etched pits, which can subsequently grow into pores. If the hole transport rate is larger than the injection rate, pores can be produced uniformly on the surface, independent of distance to the metal island structures. However, the development of a higher trench density adjacent to the metal islands, position 3/figure 3(*b*), compared to positions further away, position 1/figure 3(*a*), highlights the role of injected holes in initiating metal-assisted chemical etching at a higher rate closer to the metal islands.

3.4. Effect of catalyst on the etch rate

Previous research on metal-assisted chemical etching of Si showed that catalytic enhancement of etch rate increases in the order of Ag < Au < Pt [31–37]. Here, the catalytic enhancement of etch rate during metal-assisted chemical etching of *n*-GaN is observed to increase in the order of Ag $\leqslant$ Au < Ir < Pt, as evidenced in figure 4. Typically, metal particles exhibiting stronger catalysis produce more vigorous etching [35], which is correlated with distinctive structural features, such as helical pores [33] or rough sidewalls [25, 34]. Comparing the behavior of Ag and Au catalysts, the pore density produced using Au, figure 4(*b*), is higher than that obtained using Ag, figure 4(*a*). Ag catalyst produces a smaller number of larger pores. Although the overall etched volume of PGaN produced using Ag and Au catalysts is similar under

the processing conditions used here, they are clearly less active catalysts than Ir and Pt. Furthermore, metal-assisted chemical etching experiments employing dual metal catalysts confirm that Pt+Au is more active than Pt+Ag (figure S1 available at stacks.iop.org/SST/28/065001/mmedia). Figures 4(*c*) and (*d*) show the metal-assisted chemical etching results for Ir and Pt catalysts, respectively, with the material in each case being etched for 1/6 the time used to produce PGaN from Ag or Au. Despite being etched for a much shorter time, both Ir and Pt showed much higher pore densities and catalytic activity than Ag and Au. In addition, comparison of Pt to Ir shows that the Pt-catalyzed metal-assisted chemical etching produces larger diameter pores at roughly the same density, indicative of a faster etch rate (more material removal).

The differences in catalytic activity of Ir and Pt are also evident when *n*-GaN samples are subjected to very aggressive metal-assisted chemical etching conditions (120 min under 130 mW irradiation, not shown). Both surfaces are covered by ridge-like structures, but the width and density of ridges is clearly higher on the Ir sample than with Pt. High magnification images indicate that 20 nm diameter GaN nanowires are produced on both surfaces. A mixture of GaN particles and short nanowires are produced on the Ir catalyzed sample with a polydisperse distribution of nanowires bunched on the sidewalls of the ridges. As for the Pt-catalyzed structures, the peaks of ridges were etched effectively, leaving a porous net covered with collapsed monodisperse nanowires, with lengths averaging more than 6 μm.

A detailed explanation for the differences in catalytic activity in the metal-assisted chemical etching process is not yet clear, although a number of hypotheses have been put forward. One suggestion correlates catalytic activity with electrochemical properties [37]. The redox potential of Ag^{+}/Ag^{0} is relatively negative compared to Pt^{2+}/Pt and Au^{3+}/Au, so Ag nanoparticles can be more readily oxidized and dissolved into the H_2O_2-containing solution than Au and Pt, which have higher reduction potentials [31, 37, 38]. Although this analysis correctly predicts that Ag is the least active catalyst, it also suggests that Pt should be less active than Au, contrary to experimental observations of the metal-assisted chemical etching of *n*-GaN. Actually, Ag particles can only be slightly dissolved into the solution containing H_2O_2 [39, 40]. Furthermore, Ir is the most corrosion-resistant metal known [41], but its catalytic activity is weaker than that of Pt, as demonstrated in figure 4. Another possibility is related to the magnitude of the work functions, which increase in the order of Ag < Au < Ir < Pt [42]. Because the work functions, as shown in table 1, determine the relative amount of band bending, they affect the width of the space charge region and the ability to inject holes into the valence band. The order of the work functions predicts the order of catalytic activity correctly, and this proposition is discussed in greater detail below.

3.5. Metal shielding effects

Previously published studies of metal-assisted chemical etching of GaN use metal islands rather than continuous metal films [4, 5, 7–9]. This poses several difficulties in trying to achieve uniform morphologies or remove the residual metals without destroying the porous structures, the latter problem being particularly acute with Pt due to its insolubility. Because these residual metals can affect the quality of GaN-based devices, a protocol is sought which can effectively produce PGaN by metal-assisted chemical etching without leaving a residual film. Ag films of varied thicknesses and prepared by different protocols were loaded on the surface of *n*-GaN for metal-assisted chemical etching processing, and the results are shown in figure 5. The 3 nm Ag metal-assisted chemical etched *n*-GaN shows only slight etching, figure 5(*a*), and a high density of shallow pits. When the thickness of Ag film is increased to 20 nm, the density of the etched features decreases significantly, figure 5(*b*), a phenomenon that can be attributed to shielding of the underlying surface by the Ag catalyst. Usually, the areas around the metals are etched first in the metal-assisted chemical etching process [43, 44], and the areas underneath are protected temporarily. The 20 nm Ag film is more nearly continuous than its 3 nm counterpart, so it more effectively blocks the underlying GaN. Surprisingly, when the silver-mirror reaction, as opposed to sputtering, is used to deposit Ag, a high quality porous layer is produced after etching, as shown in figure 5(*c*). This behavior is tentatively attributed to the unique morphology of Ag metal nanoparticles produced by this method. Although the deposited films are thick, the particles produced result in a sparse coverage, allowing facile access to the underlying GaN surface [25]. This suggests a totally new method to get large-scale porous GaN layers with uniform features, which is both simple and low cost compared to the use of Pt catalysts. Furthermore, the residual can easily be removed by dipping in dilute HNO_3.

Table 1. Work function values of catalysts used in metal-assisted chemical etching.

Element	Ag[a]	Au	Ir	Pt
Work function (eV)	4.26	5.1	5.27	5.65

[a] Due to the sparing solubility of Ag nanoparticles in H_2O_2, and potential changes associated with the reaction $Ag^{+}+e^{-}_{VB} \rightarrow Ag(s)$ with $E^{0} = 0.8$ V *versus* SHE [38], the work function of Ag in solution is constrained to the range 4.26–5.06 eV.

3.6. Effect of etch time and illumination on PGaN formation with Ir catalysts

Figure 6 shows the results of a set of experiments designed to probe the effect of etch time. Given the relatively high catalytic activity of Ir, tiny pores are produced uniformly on the surface of *n*-GaN, even at the shortest etch time of 5 min, figure 6(*a*). When the etching time is increased to 30 min, uniform honeycomb-like porous structures are observed, with the structures becoming even more distinct at 45 min etch time (as shown in figure 6(*b*)), and the lengths of the pores continue to increase. Increasing the etch time to 120 min results in over-etching, as shown in figure 6(*c*). Interestingly,

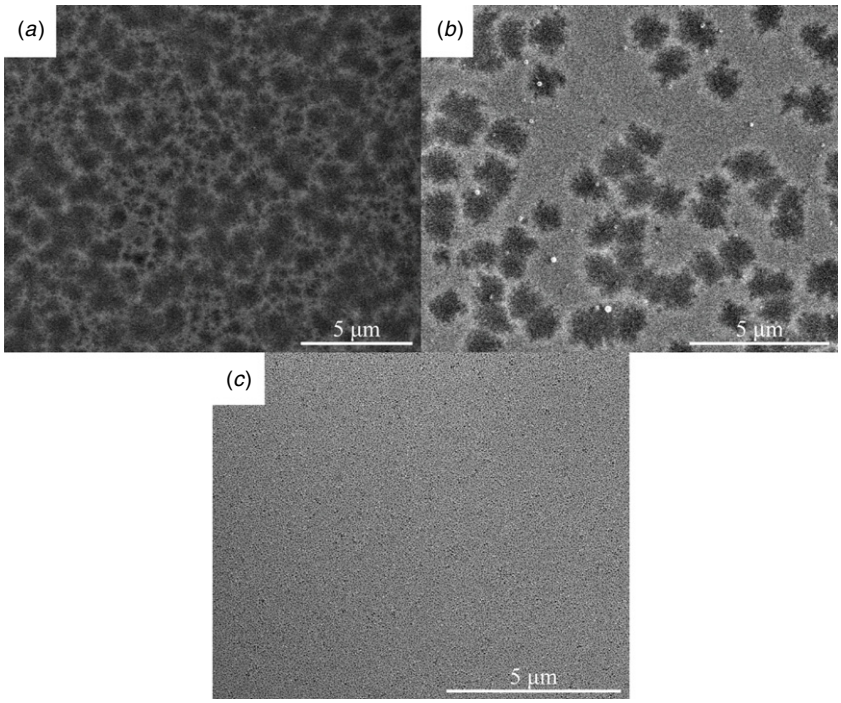

Figure 5. Top-view FESEM images of *n*-GaN wafers subjected to metal-assisted chemical etching in 2:2:1 (v:v:v) HF(49%):H_2O_2(30%): methanol at 300 K using catalytic Ag films under 130 mW UV illumination. (*a*) 3 nm sputtered film etched for 10 min; (*b*) 20 nm sputtered film etched for 10 min; and (*c*) layer deposited by silver-mirror reaction at 60 °C etched for 30 min. No special steps were taken to remove the residual metals after etching.

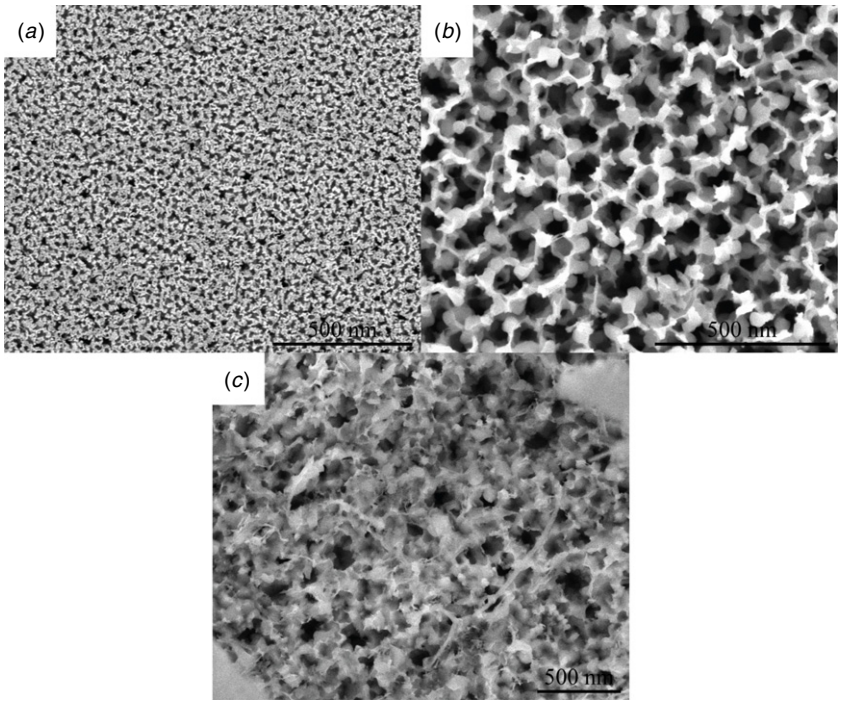

Figure 6. Top-view FESEM images of *n*-GaN wafers subjected to metal-assisted chemical etching in 2:2:1 (v:v:v) HF(49%):H_2O_2(30%): methanol at 300 K using 7 nm sputtered Ir islands under UV illumination. (*a*) 90 mW for 5 min; (*b*) 90 mW for 45 min; (*c*) 90 mW for 120 min. The observed sites correspond to position 1 in figure 1.

the over-etching is significantly improved when higher (130 mW) illumination power is used (data not shown), although the feature sizes vary with distance from the deposited patterns due to different real etching times. At the higher power, the whole surface is covered by ridge-trench structures, the formation and evolution of which has been attributed to the presence of two different etch rates, an enhanced etch rate which generates the porous network and a slower etch rate that leads to the

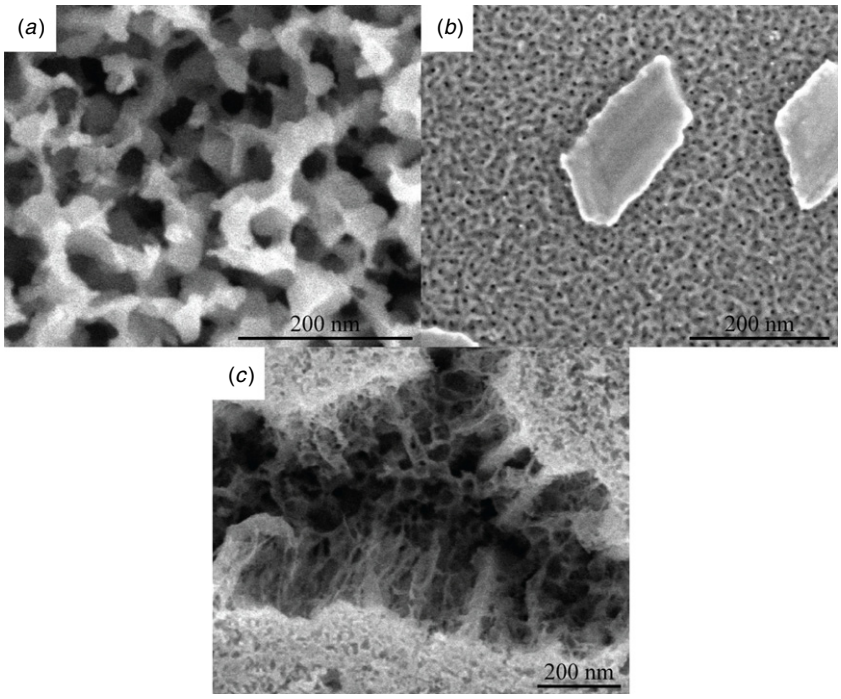

Figure 7. Top-view FESEM images of GaN wafers subjected to metal-assisted chemical etching in 2:2:1 (v:v:v) HF(49%):H_2O_2(30%): methanol at 300 K using 7 nm catalytic sputtered Ir islands under UV illumination. (*a*) *n*-GaN under 90 mW for 30 min; (*b*) *p*-GaN under 130 mW for 30 min; and (*c*) *i*-GaN under 130 mW for 30 min. The observed sites correspond to position 1 in figure 1.

terraces of the ridge morphology. The ridges might arise from grain boundaries or dislocations present in the starting GaN substrate [8].

3.7. Influence of doping type on metal-assisted chemical etching of GaN

The vast majority of reported PGaN structures produced by metal-assisted chemical etching have utilized *n*-GaN as the starting material. To understand how the intrinsic metal-assisted chemical etching activity depends on GaN doping type, *n*-type, *p*-type and intrinsic GaN were subjected to comparable metal-assisted chemical etching protocols, and the results are shown in figure 7. The metal-assisted chemical etching of *n*-GaN under 90 mW for 30 min, seen in figure 7(*a*), shows the strongly etched honeycomb structure seen previously. In contrast, *p*-GaN shows only a shallow porous layer composed of nanopores with diameters less than 10 nm, along with a small number of completely unetched features, figure 7(*b*). The intrinsic GaN in figure 7(*c*) shows metal-assisted chemical etching activity that is intermediate between the *n*- and *p*-type samples. Thus, GaN exhibits morphologies and etch rates that depend on doping type.

3.8. Relationship of metal-assisted chemical etching activity to metal-semiconductor electronic structure

Clearly the GaN doping type, together with the work function, ϕ_m, of the metal catalysts determines the detailed electronic structure of the metal–semiconductor junction formed at the catalyst–GaN interface. The metal has a much higher electron density than GaN, so the metal Fermi level and band edge profile do not change in response to the charge transfer that occurs upon contacting metal to semiconductor [27]. As shown in figure 8 and table 2, charge transfer impacts the positions of the band edges in the interfacial region and consequently, the ease with which holes can be injected into the valence band. Remembering that all energies are referenced to the vacuum level, E_{Fs}–E_{Fm} (before contact) is the critical parameter that determines the driving force for electron flow. A negative E_{Fs}–E_{Fm} before contact, as in the *n*-type material shown in figure 8(*a*), means that the semiconductor Fermi level is higher than that of the metal, indicating the electrons flow from the semiconductor into the metal, creating a Schottky barrier and an electron depletion region. The farther the value away from 0, the closer the valence band edge is, and the easier it is to inject holes into the valence band. Similarly, a positive E_{Fs}–E_{Fm} before contact, as in the *p*-type material shown in figure 8(*b*), means that the semiconductor Fermi level is lower than that of the metal, indicating the electrons flow from the metal into the semiconductor creating an electron accumulation region at the interface. The farther the value away from 0, the more difficult it is to inject holes into the valence band. Obviously, the intrinsic semiconductor displays behavior which is intermediate between these two cases.

For metal-assisted chemical etching of GaN, holes need to be excited from just above the Fermi level of the metal to the valence band, i.e. through the gap E_{vs}–E_{Fm}, leaving holes in the valence band. The smaller the E_{vs}–E_{Fm} value, the easier it is to inject holes, and the more efficient the etch process. As shown in table 2, for *n*-GaN, the gap E_{vs}–E_{Fm} decreases in the order Ag > Au > Ir > Pt, paralleling the observed order of catalytic activity. For Ag, the value of E_{Fs}–E_{Fm} can vary depending on

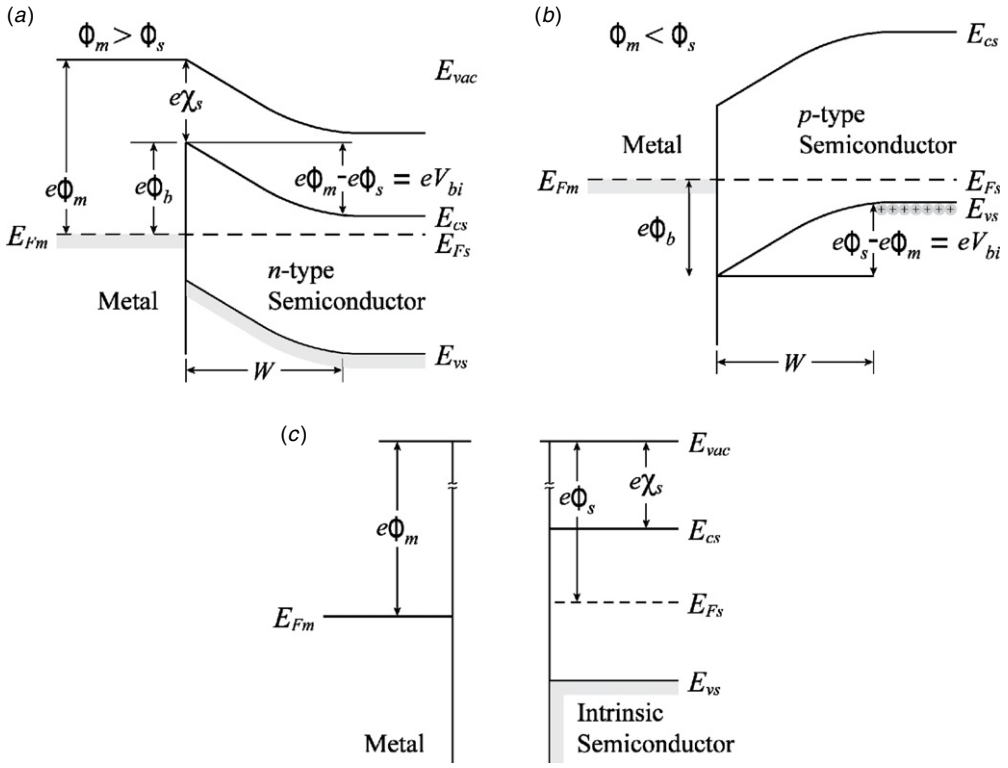

Figure 8. Schematic diagrams of ideal metal–semiconductor junctions. (*a*) The Fermi level in the semiconductor is moved as the metal is brought closer and the metal–semiconductor of *n*-type junction potential produced when the metal and semiconductor are brought together. Due to the built-in potential toward metal at the junction, a depletion region of width *W* is created. (*b*) The Fermi level in the semiconductor is moved as the metal is brought closer and the metal–semiconductor of *p*-type junction potential produced when the metal and semiconductor are brought together. The built-in potential toward semiconductor at the junction creates a depletion region of width *W*. (*c*) The positions of the energy levels in the metal and the intrinsic semiconductor. Adapted from [27].

Table 2. Values of band edge parameters for metal/gan junctions[a,b].

	n-GaN				*p*-GaN			
Element	$e\phi_b$	E_{Fs}–E_{Fm}	E_{Fs}–E_{cs}	E_{vs}–E_{Fm}	$e\phi_b$	E_{Fs}–E_{Fm}	E_{vs}–E_{Fs}	E_{vs}–E_{Fm}
Ag[c]	0.54	−0.145		3.24	2.86	3.18		3.24
		(−0.945)		(2.44)		(2.38)		(2.44)
Au	0.88	−0.985	0.015	2.4	2.52	2.34	0.06	2.4
Ir	–	−1.155		2.23	–	2.17		2.23
Pt	1.08	−1.535		1.85	2.32	1.79		1.85

	Intrinsic GaN			
Element	$e\phi_b$	E_{Fs}–E_{Fm}	E_{Fs}–E_{cs}	E_{vs}–E_{Fm}
Ag[c]	–	1.54	1.7	3.24
(0.74)				
Au	–	0.7		2.4
Ir	–	0.53		2.23
Pt	–	0.15		1.85

[a] All values given in eV.

[b] Values listed for E_{Fs}–E_{Fm} and E_{Fs}–E_{cs} are given prior to contact. E_{Vs}–E_{Fm} values are after contact.

[c] As in table 1, the values related to Ag vary. The values of E_{Fs}–E_{Fm} and E_{vs}–$E_{Fm}$for Ag^+ solution in contact with Ag are given in brackets, but the actual values are closer to pure Ag. The values of E_{Fs}–E_{cs} (before contact) of *n*-GaN and E_{vs}–E_{Fs} (before contact) of *p*-GaN were calculated from [27],

$$E_F = E_C + kT\left[\ln\frac{n}{N_C} + \frac{n}{\sqrt{8}N_C}\right] = E_V - kT\left[\ln\frac{p}{N_V} + \frac{p}{\sqrt{8}N_V}\right].$$

the degree of dissolution of Ag to produce Ag^+. Thus, E_{Fs}–E_{Fm} is stated as a range for Ag, e.g. −0.945 to −0.145 eV for *n*-GaN. Meanwhile, the built-in potential tends to repel the holes to the surface of semiconductor, facilitating collection of holes at the right physical location to participate in reaction (2) and contribute to etching. It should also be noted that, in principle, there is a small contribution to the etching from direct bandgap excitation of electron–hole pairs with UV irradiation with energies above the bandgap. Indeed, figure 2(*a*) shows a small amount of etching in the absence of catalyst, which would have to involve direct excitation of carriers.

In contrast, the interface of metal with *p*-GaN is characterized by an electron accumulation (hole depletion) region, figure 8(*b*), meaning that a drift force exists in the interfacial region driving holes into the bulk and away from the interface where they need to take part in reaction (2). Thus, *p*-GaN should exhibit lower metal-assisted chemical etching rates than *n*-GaN, as is clearly observed, cf figures 7(*a*) and (*b*). In addition, the values of E_{Fs}–E_{Fm} before contact are consistent with this interpretation, being large and positive for all four metals studied, meaning that a large barrier to hole injection exists at the metal–semiconductor interface. In intrinsic GaN, the Fermi level lies near the middle of the bandgap, and the values of E_{Fs}–E_{Fm} of the junctions are intermediate between those of *n*-GaN and *p*-GaN. Quantitative consideration of the band offsets, however, shows that they are positive as they are in *p*-GaN, which means a small electron accumulation region is formed at the interface, as in *p*-GaN, mitigating against hole transport to the semiconductor solution interface. Therefore, intrinsic material is more active to metal-assisted chemical etching than *p*-GaN, but not as active as *n*-GaN.

Finally, we note that the metal-assisted chemical etching activity of GaN increases in the order *p*-GaN < intrinsic GaN < *n*-GaN due to the electronic structure factors discussed above. This is different from the metal-assisted chemical etching of Si, which is characterized by a much narrower bandgap than GaN, thus altering the work function and the associated band edge offsets prior to contact, table S2 available at stacks.iop.org/SST/28/065001/mmedia.

4. Conclusion

The influence of catalyst on the morphologies of *n*-GaN subjected to metal-assisted chemical etching shows that the catalytic activity increases in the order of Ag < Au < Ir < Pt. Using Ag or Au sputtered films, only shallow pores are formed on the surface of GaN under the UV-irradiation. Uniform porous layers evolve gradually by increasing the illumination power or increasing the etching time when Ir or Pt are used as catalysts. Continuous metal films effectively shield the underlying GaN from etching, a problem that can be addressed by preparing sparse Ag films, for example, through the silver-mirror reaction. In the metal-assisted chemical etching of GaN, the key step is identified as the hole generation by catalytic reduction of H_2O_2 and subsequent hole injection into the valence band with the aid of UV irradiation. In *n*-GaN, the barrier to hole injection is dependent on the identity of the catalyst. Different metals with different work functions evince different initial band offsets, E_{vs}–E_{Fm}, which correlate with the magnitude of the barrier to hole injection. For *n*-GaN, E_{vs}–E_{Fm} decreases in the order Ag > Au > Ir > Pt, which is the inverse order of catalytic activity. The doping type has an even larger effect on the etch rate, which increases in the order of *p*-GaN < intrinsic GaN < *n*-GaN, an observation that is explained by a combination of (*a*) different barriers to hole injection and (*b*) the formation of an electron accumulation (hole depletion) region at the interface for *p*-GaN and intrinsic material, and an electron depletion (hole accumulation) region for *n*-GaN. The results reported in this paper are relevant to the design of devices incorporating PGaN inasmuch as they identify the material properties (doping type, catalyst identity) and processing conditions (irradiation, etch times) that are most effective in yielding a highly active metal-assisted chemical etching.

Acknowledgment

This work was supported by the US National Science Foundation through grant NSF1111739 (support of XG), the US Department of Energy grant DE FG02 07ER15851 (support of DAG) and the US Army under contract W9132T-07-2-0003 (support of BKD). The authors gratefully acknowledge the Notre Dame Integrated Imaging Facility for assistance with the electron microscopy, and Chaoxiong Ma for valuable discussions.

References

[1] Shul R J, Kilcoyne S P, Crawford M H, Parmeter J E, Vartuli C B, Abernathy C R and Pearton S J 1995 High-temperature electron-cyclotron-resonance etching of Gan, Inn, and Aln *Appl. Phys. Lett.* **66** 1761–3

[2] Vajpeyi A P, Chua S J, Tripathy S and Fitzgerald E A 2007 Effect of carrier density on the surface morphology and optical properties of nanoporous GaN prepared by UV assisted electrochemical etching *Appl. Phys. Lett.* **91** 083110

[3] Al-Heuseen K, Hashim M R and Ali N K 2011 Growth and characterization of tree-like crystalline structures during electrochemical formation of porous GaN *J. Electrochem. Soc.* **158** D240–3

[4] Duan B K and Bohn P W 2010 High sensitivity hydrogen sensing with Pt-decorated porous gallium nitride prepared by metal-assisted electroless etching *Analyst* **135** 902–7

[5] Yam F K and Hassan Z 2009 Structural and optical characteristics of porous GaN generated by electroless chemical etching *Mater. Lett.* **63** 724–7

[6] Ng H M, Weimann N G and Chowdhury A 2003 GaN nanotip pyramids formed by anisotropic etching *J. Appl. Phys.* **94** 650–3

[7] Diaz D J, Williamson T L, Adesida I, Bohn P W and Molnar R J 2002 Morphology and luminescence of porous GaN generated via Pt-assisted electroless etching *J. Vac. Sci. Technol.* B **20** 2375–83

[8] Diaz D J, Williamson T L, Adesida I, Bohn P W and Molnar R J 2003 Morphology evolution and luminescence properties of porous GaN generated via Pt-assisted electroless etching of hydride vapor phase epitaxy GaN on sapphire *J. Appl. Phys.* **94** 7526–34

[9] Li X L, Kim Y W, Bohn P W and Adesida I 2002 In-plane bandgap control in porous GaN through electroless wet chemical etching *Appl. Phys. Lett.* **80** 980–2

[10] Kaminska A *et al* 2011 Highly reproducible, stable and multiply regenerated surface-enhanced Raman scattering substrate for biomedical applications *J. Mater. Chem.* **21** 8662–9

[11] Vajpeyi A P, Chua S J, Tripathy S, Fitzgerald E A, Liu W, Chen P and Wang L S 2005 High optical quality nanoporous GaN prepared by photoelectrochemical etching *Electrochem. Solid State Lett.* **8** G85–8

[12] Ryu S W, Zhang Y, Leung B, Yerino C and Han J 2012 Improved photoelectrochemical water splitting efficiency of nanoporous GaN photoanode *Semicond. Sci. Technol.* **27** 015014

[13] Yam F K and Hassan Z 2007 Schottky diode based on porous GaN for hydrogen gas sensing application *Appl. Surf. Sci.* **253** 9525–8

[14] Chiu S Y, Huang H W, Liang K C, Huang T H, Liu K P, Tsai J H and Lour W S 2009 High sensing response Pd/GaN hydrogen sensors with a porous-like mixture of Pd and SiO2 *Semicond. Sci. Technol.* **24** 045007

[15] Wang X H, Wang X L, Feng C, Yang C B, Wang B Z, Ran J X, Xiao H L, Wang C M and Wang J X 2008 Hydrogen sensors based on AlGaN/AIN/GaN HEMT *Microelectron. J.* **39** 20–3

[16] Eickhoff M, Ambacher O, Steinhoff G, Schalwig J, Neuberger R, Palacios T, Monroy E, Calle F, Müller G and Stutzmann M 2001 Novel sensor applications of group-III nitrides *Proc. MRS* **693** I12.1.1

[17] Dylewicz R, Khokhar A Z, Wasielewski R, Mazur P and Rahman F 2011 Nanotexturing of GaN light-emitting diode material through mask-less dry etching *Nanotechnology* **22** 055301

[18] Al-Heuseen K, Hashim M R and Ali N K 2011 Effect of different electrolytes on porous GaN using photo-electrochemical etching *Appl. Surf. Sci.* **257** 6197–201

[19] Cho H, Auh K H, Han J, Shul R J, Donovan S M, Abernathy C R, Lambers E S, Ren F and Pearton S J 1999 UV-photoassisted etching of GaN in KOH *J. Electron. Mater.* **28** 290–4

[20] Pearton S J, Zolper J C, Shul R J and Ren F 1999 GaN: processing, defects, and devices *J. Appl. Phys.* **86** 1–78

[21] Zhang Y, Ryu S W, Yerino C, Leung B, Sun Q A, Song Q H, Cao H and Han J 2010 A conductivity-based selective etching for next generation GaN devices *Phys. Status Solidi* B **247** 1713–6

[22] Li X and Bohn P W 2000 Metal-assisted chemical etching in HF/H2O2 produces porous silicon *Appl. Phys. Lett.* **77** 2572–4

[23] Yasukawa Y, Asoh H and Ono S 2008 Site-selective chemical etching of GaAs through a combination of self-organized spheres and silver particles as etching catalyst *Electrochem. Commun.* **10** 757–60

[24] Williamson T L, Diaz D J, Bohn P W and Molnar R J 2004 Structure–property relationships in porous GaN generated by Pt-assisted electroless etching studied by Raman spectroscopy *J. Vac. Sci. Technol.* B **22** 925–31

[25] Geng X W, Li M C, Zhao L C and Bohn P W 2011 Metal-assisted chemical etching using Tollen's reagent to deposit silver nanoparticle catalysts for fabrication of quasi-ordered silicon micro/nanostructures *J. Electron. Mater.* **40** 2480–5

[26] Yeh Y H, Hsu Y C, Wu Y H, Chen K M and Lee W I 2011 Hydrogen etch of GaN and its application to produce porous GaN caves *Gallium Nitride Mater. Devices VI* **7939** 79390P

[27] Umesh K and Mishra J S 2008 *Semiconductor Device Physics and Design* (Dordrecht: Springer)

[28] Levinshtein M E, Rumyantsev S L and Shur M S 2001 *Properties of Advanced Semiconductor Materials: GaN, AlN, InN, BN, SiC, SiGe* (New York: Wiley)

[29] Cerofolini G F 1998 A study of the ionic route for hydrogen terminations resulting after SiO2 etching by concentrated aqueous solutions of HF *Appl. Surf. Sci.* **133** 108–14

[30] Housecroft C E and Sharpe A G 2001 *Inorganic Chemistry* (New York: Prentice Hall)

[31] Chartier C, Bastide S and Levy-Clement C 2008 Metal-assisted chemical etching of silicon in HF-H_2O_2 *Electrochim. Acta* **53** 5509–16

[32] Cruz S, Honig-dOrville A and Muller J 2005 Fabrication and optimization of porous silicon substrates for diffusion membrane applications *J. Electrochem. Soc.* **152** C418–24

[33] Megouda N, Hadjersi T, Piret G, Boukherroub R and Elkechai O 2009 Au-assisted electroless etching of silicon in aqueous HF/H(2)O(2) solution *Appl. Surf. Sci.* **255** 6210–6

[34] Peng K Q and Zhu J 2004 Morphological selection of electroless metal deposits on silicon in aqueous fluoride solution *Electrochim. Acta* **49** 2563–8

[35] Tsujino K and Matsumura M 2005 Boring deep cylindrical nanoholes in silicon using silver nanoparticles as a catalyst *Adv. Mater.* **17** 1045–7

[36] Yae S, Tanaka H, Kobayashi T, Fukumuro N and Matsuda H 2005 Porous silicon formation by HF chemical etching for antireflection of solar cells *Phys. Status Solidi C– Conf. Crit. Rev.* **2** 3476–80

[37] Lee C L, Tsujino K, Kanda Y, Ikeda S and Matsumura M 2008 Pore formation in silicon by wet etching using micrometre-sized metal particles as catalysts *J. Mater. Chem.* **18** 1015–20

[38] Peng K Q, Lu A J, Zhang R Q and Lee S T 2008 Motility of metal nanoparticles in silicon and induced anisotropic silicon etching *Adv. Funct. Mater.* **18** 3026–35

[39] Maggs F T and Sutton D 1958 Some aspects of the catalytic decomposition of concentrated hydrogen peroxide by silver: 1. The solubility and rate of solution of silver *Trans. Faraday Soc.* **54** 1861–70

[40] Maggs F T and Sutton D 1959 Some aspects of the catalytic decomposition of concentrated hydrogen peroxide by silver: 2. Electrical conductivity and Ph of solutions of hydrogen peroxide containing silver *Trans. Faraday Soc.* **55** 974–80

[41] Emsley J 2011 *Nature's Building Blocks: An A–Z Guide to the Elements* (Oxford: Oxford University Press)

[42] Michaelson H B 1977 Work function of elements and its periodicity *J. Appl. Phys.* **48** 4729–33

[43] Chattopadhyay S, Li X L and Bohn P W 2002 In-plane control of morphology and tunable photoluminescence in porous silicon produced by metal-assisted electroless chemical etching *J. Appl. Phys.* **91** 6134–40

[44] Geng X W, Duan B K, Grismer D A, Zhao L C and Bohn P W 2012 Monodisperse GaN nanowires prepared by metal-assisted chemical etching with *in situ* catalyst deposition *Electrochem. Commun.* **19** 39–42